Supporting Information for "Ultrafast 2D-IR spectroscopy of [NiFe] hydrogenases reveals the role of the protein scaffold in controlling the active site environment"

Solomon L.D. Wrathall,[1†] Barbara Procacci,[1†] Marius Horch,[2] Emily Saxton,[1] Chris Furlan,[1] Julia Walton,[1] Yvonne Rippers,[2] James N. Blaza,[1] Gregory M. Greetham,[3] Michael Towrie,[3] Anthony W. Parker,[3] Jason Lynam,[1] Alison Parkin[1*] and Neil T. Hunt[1*]

Contents

Materials and Methods

Purification of *E. coli* hydrogenase-1 (*Ec*Hyd-1)

The protein preparation protocol is modified from Flanagan et al.[1]

Growth

E. coli cells (derived from a K12 parent strain, LF03 mutant) featuring a His_6 tag at the 3'-terminus of the gene encoding the Hyd-1 small subunit (HyaA) were grown as reported previously to yield 3 or 4 x 6L cultures.[1]

Isolation

The cell harvesting, lysis and solubilisation of *Ec*Hyd-1 from the membrane was carried out with the following two modifications to the previously published[1] protocol: (i) After the lysis of cells by osmotic shock, the solution used for the overnight solubilisation of membrane proteins contained 3% (w/v) Triton X-100 (rather than 9%), and 500 µM AEBSF, 50 µM leupeptin and 1 µM pepstatin (rather than adding cOmplete™ EDTA-free protease inhibitor tablets); (ii) After the pelleting of cell debris by centrifugation, the supernatant was adjusted to 30 mM imidazole (rather than 50 mM).

Purification

*Ec*Hyd-1 was purified using a 5 mL HisTrap column (GE Life Sciences) as described previously,[1] but with the following two modifications: (i) Elution buffer A comprised: 30 mM imidazole, 150 mM NaCl, 100 mM Tris, pH 7.6 (rather than 50 mM imidazole, 150 mM NaCl, 100 mM Tris, pH 7.6), and buffer B comprised 500 mM imidazole, 150 mM NaCl, 100 mM Tris, pH 7.6 (rather than 1 M imidazole, 150 mM NaCl, 100 mM Tris, pH 7.6); (ii) Hydrogenase containing fractions were exchanged into imidazole-free buffer and concentrated using a 30 kDa MWCO centrifugal concentrator (Vivaspin 20, GE Healthcare) on the same day as running the Ni-column (rather than using overnight dialysis and centrifugal concentration the following day).

Post purification, the total protein content of samples was determined with the Coomassie (Bradford) Protein Assay using bovine serum albumin (BSA) as calibrant.

IR absorption, IR pump-IR probe and 2D-IR spectroscopy

Infrared spectroscopy experiments on *Ec*Hyd-1 (in buffer comprising: 150 mM NaCL, 100 mM Tris, pH 7.6) were conducted using cells featuring CaF_2 windows and a PTFE spacer that gave an optical pathlength of 50 µm. For 2D-IR experiments on the enzyme, a gas-tight small volume (15 µL) sandwich cell was used, whereas a Harrick cell was used for the gas-exchange FT-IR experiments

IR absorption spectra were recorded in transmission mode at room temperature using a Bruker Vertex 70 spectrometer with a frequency resolution of 2 cm^{-1}. The empty spectrometer was used as a background. Spectra were averaged over 400 scans, before fitting and subtracting a polynomial baseline over the region 1850 to 2150 cm^{-1} to remove the effects of absorptions due to the solvent.

Simulating 2D-IR spectra

Each individual peak was simulated using the 2D-Gaussian equation shown in (equation 1) and summed to generate full spectra.[2]

$$f(x,y) = A \exp\left[-\frac{1}{2\left(1-{C_{2D}}^2\right)}\left(\left(\frac{x-x_0}{\sigma_x}\right)^2+\left(\frac{y-y_0}{\sigma_y}\right)^2-\frac{2C_{2D}(y-x_0)(x-y_0)}{\sigma_y\sigma_x}\right)\right] \quad (1)$$

Where:

f(x,y) = signal amplitude at pump wavenumber, probe wavenumber of (x,y)

x= probe wavenumber

y= pump wavenumber

A = amplitude of peak

C_{2D} =cross correlation parameter

x_0 = central wavenumber of peak along probe axis

y_0 = central wavenumber of peak along probe axis

σ_x = standard deviation along probe axis

σ_y = standard deviation along pump axis

$$\sigma_x = \frac{FWHM_x}{2\sqrt{2\,ln(2)}} \quad (2)$$

Protein characterisation methods

Gas cycling experiments

Approximately 25 µL of as-isolated *Ec*Hyd-1, pH 7.6, was used to fill a Harrick cell and IR absorption spectra were collected ("As-isolated" data in Figure 1(b) of main paper). Gas cycling experiments were then performed on the same sample of enzyme by first porting a 75 µL aliquot of *Ec*Hyd-1 into a glovebox (Faircrest, O_2 < 10 ppm) and exposing it to an active flow of 100% H_2 for 2 hours and then leaving the enzyme under a quiescent 100% H_2 atmosphere for 18 hours at 4 °C. The Harrick IR cell was then filled (approx. 25 µL) with H_2-exposed *Ec*Hyd-1 inside the glovebox, before it was ported out and the FT-IR was recorded ("Reduced" data in Figure 1(b) of main paper). A 25 µL aliquot of the H_2-saturated *Ec*Hyd-1 was then ported out of the glovebox and exposed to a flow of 100% O_2 for 1 hour at room temperature. The FT-IR absorption spectra of this sample were then recorded and processed using the same method as described above ("Oxidised" data in Figure 1(b) of main paper).

Cryo-electron microscopy (cryo-EM)

Prior to cryo-electron microscopy, *Ec*Hyd-1 was subject to a second purification step via size exclusion chromotography. 1.2/1.3 UltrAuFoil grids were glow discharged (PELCO easiGlow) for 90 s on each side using atmospheric gas before mounting in Vitrobot tweezers. 1 mg mL^{-1} Hyd-1 aliquots were defrosted and 2.5 µL placed onto the grid, blotted (4°C, 100% humidity), and plunged into liquid ethane. Blot time was 3 s and blot force was constant at -5.

Data collection was performed on a Glacios microscope operated at 200 kV. One exposure was collected per hole, and the autofocus routine was run every 10 µm. A nominal magnification of 120K, spot size of 6, illuminated area of 1 µm were used and data were collected at a calibrated pixel size of 1.2 Å. The total fluence was of 50.0 electrons/ $Å^2$. A total of 921 EER movies were collected.

The Relion pipeline was used for all image processing. Whole micrograph motion correction and damage weighting were performed using the implementation of MotionCor2 in Relion. Initial CTF values were determined with CTFFIND4 and the Laplacian-of-Gaussian (LoG) filter was used to select an initial set of particles. 2D classification was used in multiple rounds. The datasets led to two classes, indicating strong preferred orientation.

H_2-oxidation solution activity assay

Hydrogen oxidation kinetics were monitored spectrophotometrically at room temperature via the reductive decolourisation of methylene blue inside a glove box (Faircrest, O_2 < 10 ppm).[3,4] First, the extinction coefficient at approx. 626 nm of fully oxidised methylene blue was determined by measuring the absorbance of methylene blue solutions of different concentration (0, 2, 5, 8, 10, 14, 22 and 25 µM) in mixed buffer (15 mM MES, CHES, TAPS, HEPES and Na acetate at pH 7.6) using a custom-built spectrophotometer containing a narrow band LED.[1] Then, a 2 mL aliquot of H_2-saturated solution containing 25 µM methylene blue in mixed buffer (pH 7.6) was injected into a cuvette (polystyrene, 3 mL volume, 10 mm optical path length, Fisher) through a subaseal-lid. To the cuvette was added 10 µL of enzyme solution. The cuvette was placed inside the custom-built spectrophotometer. The H_2-oxidation activity was monitored via the concomitant reduction of methylene blue.

Cyclic voltammetry (CV) experiments

Electrochemical experiments were performed in a similar manner to those described previously.[3] A glovebox (Faircrest, O_2 < 10 ppm) with a three-electrode setup featuring a saturated calomel reference, platinum counter and pyrolytic graphite edge (PGE) working electrode (0.03 cm^{-2} geometric disk area) was used. Experiments were performed using a water-jacketed, gas-tight glass electrochemical cell filled with mixed buffer comprising 15 mM, MES, CHES, TAPS, HEPES and Na acetate at pH 7.6. The temperature of the cell was maintained at 30°C using a water circulator and the atmosphere maintained with a flow of approximately 1 cm^3 s^{-1} of 100% H_2 gas. The (PGE) electrode surface was prepared by abrasion with sandpaper (Norton) before application of 2 µL of 20 µM enzyme solution, the enzyme was left to adhere to the surface for approximately 30 s before rinsing off the excess using 200 µL of buffer. The working electrode was rotated at 3000 rpm using an Origatrod rotator

(Origalys) to ensure that catalysis was not rate limited by mass transport of substrate/product. Measurements were performed using an Ivium CompactStat potentiostat and with IviumSoft software.

Native-PAGE

Precast Native-PAGE gels (Bio-Rad Mini-PROTEAN® TGX™) were run and either stained using Coomassie blue to reveal all protein bands, or transported into a glove box (Faircrest, O_2 < 10 ppm) and placed overnight in a sealed box containing H_2-saturated buffer comprising 50 mM potassium phosphate (pH 7.6), 90 µM phenazine methosulfate and 60 µM nitroblue tetrazolium. Active hydrogenase present in gel bands oxidises H_2 and transmits electrons via phenazine carrier molecules to the nitroblue blue tetrazolium dye, ensuring only protein bands that contain active hydrogenase are stained.[2]

Characterization of *Ec*Hyd-1

Comparing FT-IR of as-isolated EcHyd-1 from different protein purifications

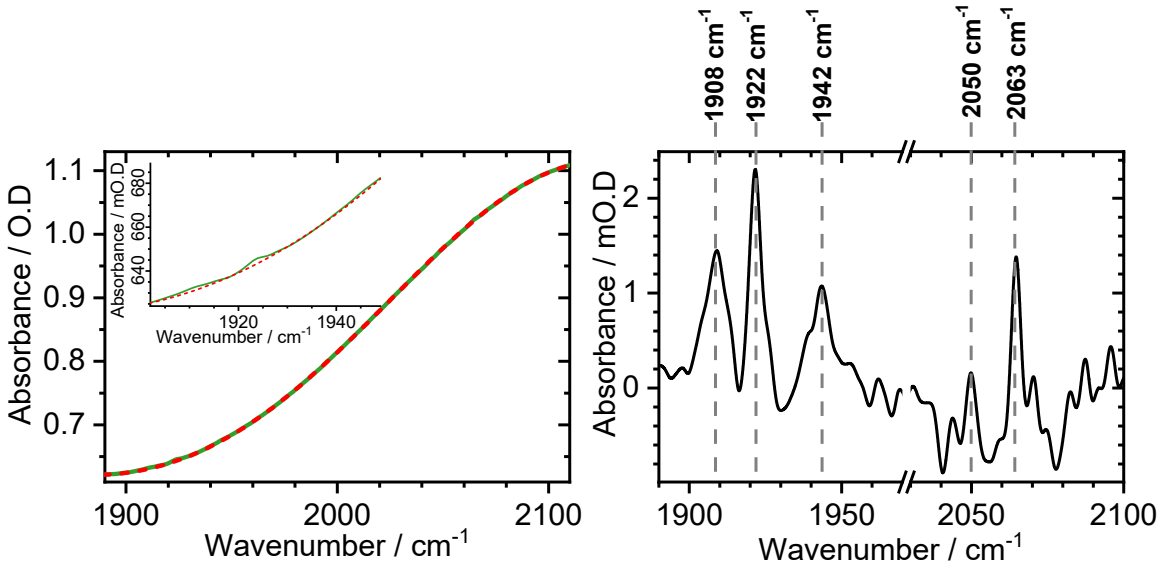

Figure S1: (a) FT-IR spectrum of *Ec*Hyd-1 sample used in pump-probe and 2D-IR experiments, showing absorbance spectrum (solid green line) and polynomial baseline (red dashed line), with an inset that provides an expanded view of the ν_{CO} region. **(b)** FT-IR spectrum following baseline subtraction.

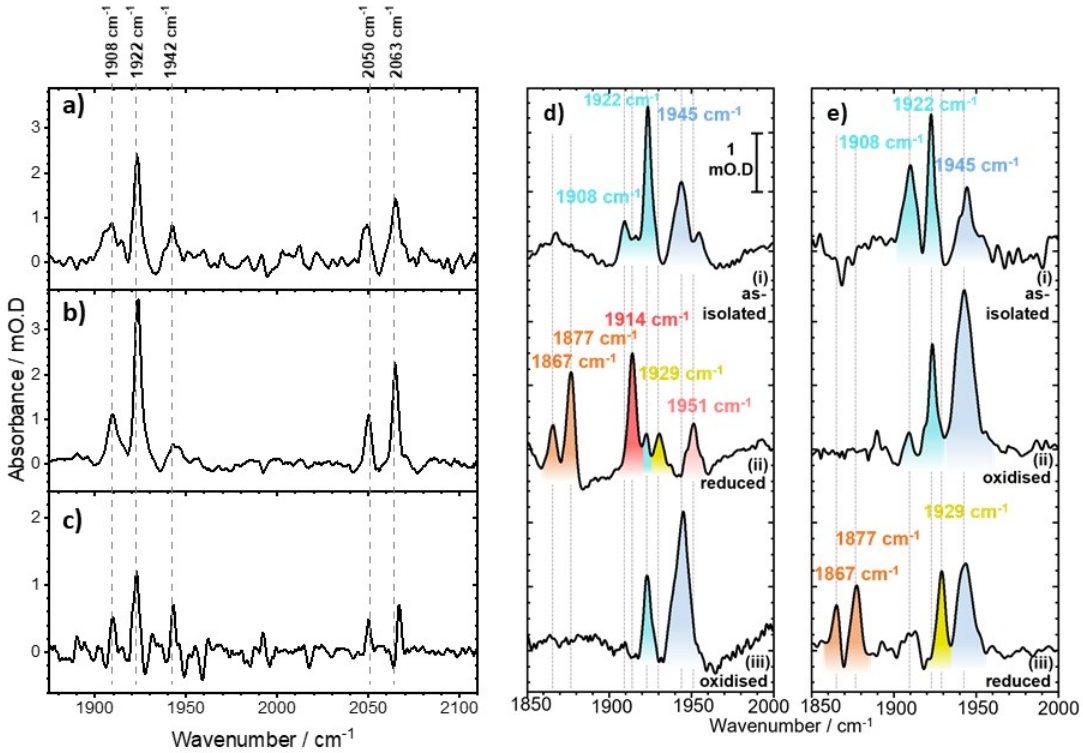

Figure S2: (a-c) FT-IR spectra of *Ec*Hyd-1 samples from three different cell growth and protein purification processes. This data indicates that the results shown in Figure S1 are consistent across multiple experiments. The sample analysed in a) was also used in the H_2-oxidation activity assays. (d-e) IR absorption (FT-IR) spectra of EcHyd-1 in the ν_{CO} region of the spectrum, enzyme samples were exposed to differing gas atmospheres (i-iii) and exposure orderings (d-e). In (d) the as-isolated EcHyd-1 sample (i) was H_2-reduced (ii) and subsequently O_2-oxidised (iii). In (e) the as-isolated EcHyd-1 sample (i) was O_2-oxidised (ii) and subsequently H_2-reduced (iii). Coloured labels indicate the wavenumbers of bands due to carbonyl stretching modes and the color scheme is consistent with that in Figure 1(a) in the main text.

Analysis of the oligomeric states of EcHyd-1

As-isolated samples of *Ec*Hyd-1 were analysed with cryo-electron microscopy (cryo-EM). The samples used were not the same as those used for 2D-IR experiments, although they were produced according to the same protocol and the PAGE (Figure S3(f)) and FT-IR data (Figure S6(b)) indicates that they are equivalent. While the orientational bias of particles on the cryo-EM grids prevented attainment of a high-resolution structure, the resolution was sufficient to confirm that the arrangement of subunits matches that of previously-reported X-ray crystallographic data for the $(HyaAHyaB)_2$ dimer-of-dimers.[6]

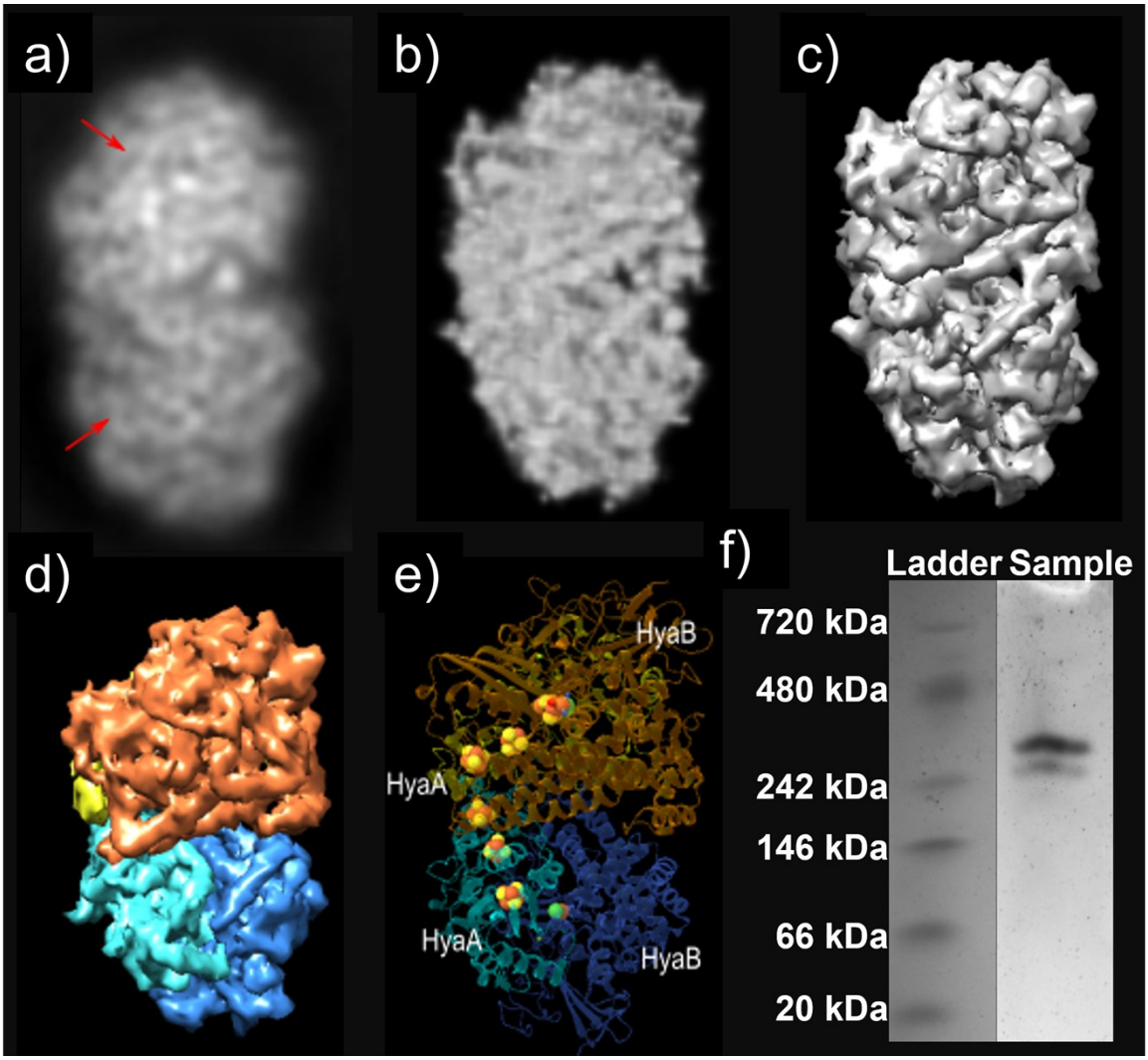

Figure S3: (a) EcHyd-1 2D class obtained from the cryo-EM data using RELION 3.1, **(b)** solid map created using existing crystallographic structures showing the similarity to the 2D experimental class, **(c)** 3D display of the solid map in panel b, **(d)** panel c but with coloured subunits, **(e)** ribbon structure used to create the maps shown in panels b, c, d **(f)** Native PAGE of the *Ec*Hyd-1 sample used for cryo-EM measurements.

To probe the oligomeric state of our as-isolated *Ec*Hyd-1 enzyme, Native-PAGE gels with Coomassie and H_2-oxidation staining were run on the *Ec*Hyd-1 sample used for the 2D-IR experiments reported in the main paper, as summarised in Figure S4. These experiments show that the band with maximal H_2 oxidation activity runs at a mass in the 242-280 kDa range which is consistent with a dimer of heterodimers of large (HyaB) and small (HyaA) subunits of *Ec*Hyd-1, i.e. $(HyaAHyaB)_2$, which should have a mass of 205 kDa.

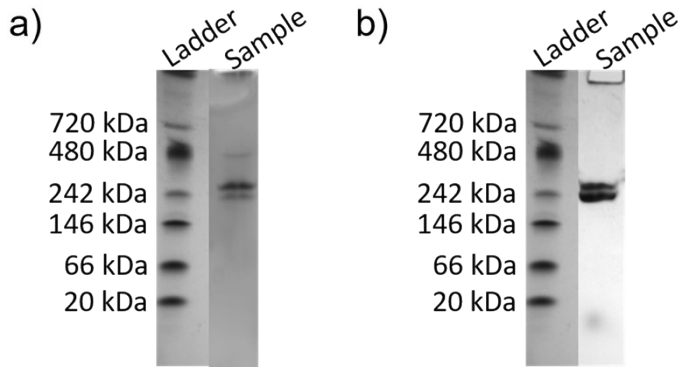

Figure S4: Native-PAGE gel resolution of an as-isolated *Ec*Hyd-1 sample, with **(a)** Coomassie staining, and **(b)** in-gel H_2-oxidation activity staining. The same ladder is replicated twice to assist in visual analysis of the data.

Methylene blue H_2-oxidation activity assay

The H_2-oxidation activity of "as-isolated" and H_2-saturated *Ec*Hyd-1 samples was compared using a methylene blue assay (Figure S5), using a method reported in our previous work and detailed above.[3] The protein samples tested were not from the same purification run as those used for 2D-IR, although FT-IR confirmed a similar distribution of states in the as-purified samples (compare Figure S1 which shows FT-IR of the 2D-IR enzyme sample and Figure S2(c) which shows FT-IR of the enzyme sample used for the assay measurements).

Based on the solution activity assay data (Figure S5), a sample turnover rate of 6.3 ± 0.2 s^{-1} is determined for as-isolated *Ec*Hyd-1 when the Bradford assay measurement of total protein concentration is used as a proxy for the total hydrogenase concentration. Pre-activating an aliquot of the same protein sample by exposure to a 100% H_2-atmosphere (see above for methodology) results in an increase in the turnover rate to 48.7 ± 0.6 s^{-1} at pH 7.6, and this value is comparable to previous measurements reported for H_2-saturated *Ec*Hyd-1 (approximately 65 s^{-1} at pH 6.0,[3] and 21 ± 4 s^{-1} at pH 4.5[1]).[1,3]

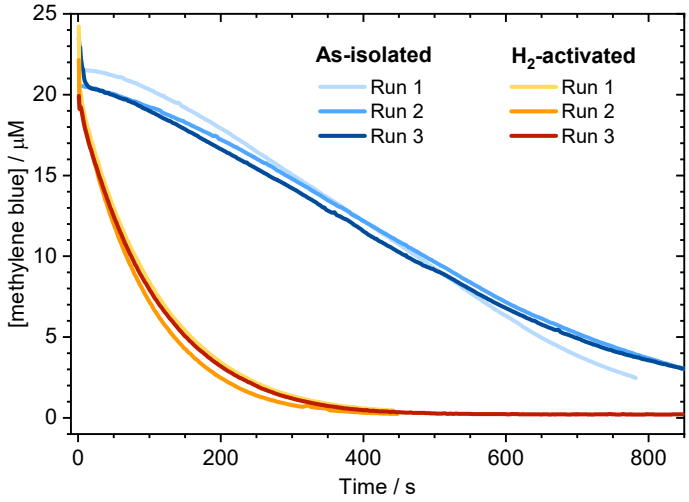

Figure S5: Solution activity assay data, showing the H_2-oxidation activity of *Ec*Hyd-1 determined via the reduction of methylene blue (MB^+), monitored spectrophotometrically. Data are shown for as-isolated enzyme (blue) and for samples that had been pre-activated by exposure to a 100% H_2-atmosphere for 2 h (yellow-red). The reported turnover rate (k_{cat}) represents the average of three repeats.

Reactivation kinetics monitored by cyclic voltammetry

The timescale by which molecules of as-isolated and O_2-inhibited *Ec*Hyd-1 were converted to their fully active forms was monitored in cyclic voltammetry experiments as described in the main paper and shown in Figure S6. The protein samples used were not the same as those used for 2D-IR experiments, although they were produced according to the same protocol.

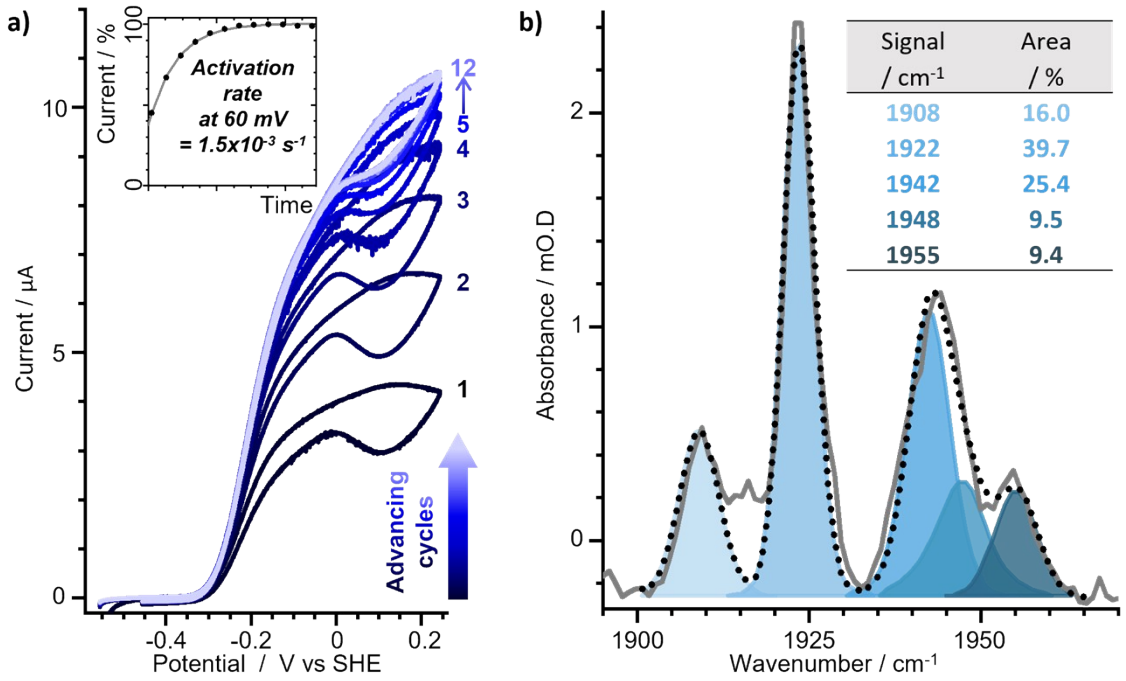

Figure S6: As-isolated *Ec*Hyd-1 **(a)** cyclic voltammograms with inset current/time plot showing the activation rates, and **(b)** FT-IR spectra (solid grey trace) fitted to Gaussian functions (dotted black for cumulative fit) with inset tables showing the integral areas for each state.

Spectroscopic analysis

The potential energy of an anharmonic diatomic molecule is described by the Morse potential as a function of bond length (r), equilibrium bond length (r_e), well depth (D_e) and curvature of the well (a) in (equation 1).

$$V'(r) = D_e\left(1 - e^{-a(r - r_e)}\right)^2 \qquad (1)$$

Approximate solutions to the Morse potential can be obtained from (equation 2) which alternatively be expressed as (equation 3).

$$E_n = h\nu_0\left(n + {}^1/_2\right) - \frac{1}{4D_e}\left[h\nu_0\left(n + {}^1/_2\right)\right]^2 \qquad (2)$$

$$v_{n \to n+1} = -\frac{nhv_0^2}{2D_e} + v_0 - \frac{hv_0^2}{2D_e} \qquad (3)$$

Alternatively, the vibrational energy levels of an anharmonic diatomic molecule can be given by the empirical expression shown in (equation 4).

$$E_n = hv_0\left(n + {}^1\!/_2\right) - hv_0\chi_e\left(n + {}^1\!/_2\right)^2 \qquad (4)$$

Combining (equation 2) and (equation 4) allows determination of the anharmonicity constant (X_e) as in (equation 5).

$$\chi_e = \frac{hv_0}{4D_e} \qquad (5)$$

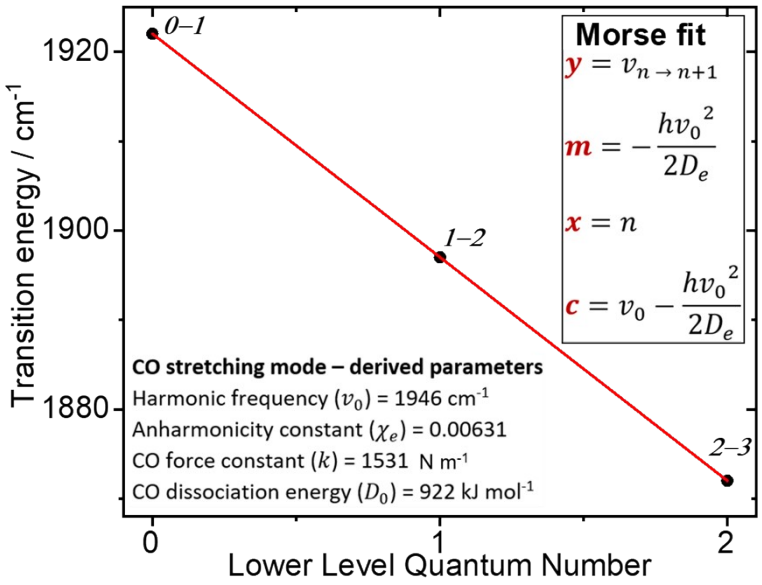

Figure S7: Transition energies for the CO stretching mode of *Ec*Hyd-1 with a v=0-1 frequency of 1922 cm^{-1}. The results were determined by fitting a linear function (red line) representing the energy level separations of a Morse potential to the experimental data (black dots). Transitions between vibrational energy levels (n → n+1) are labelled as *v=n-n+1*.

Table S1: Morse fitting parameters determined for the CO stretching vibrational modes of three active site states of *Ec*Hyd-1 with fundamental frequencies of 1908, 1922 and 1945 cm^{-1}. (± values indicate standard deviation derived from fitting).

CO stretch (v=0-1) / cm^{-1}	1908	1922	1942
CN stretch 2 (v=0-1) / cm^{-1}	2057	2050	2080
CN stretch 1 (v=0-1) / cm^{-1}	2070	2063	2092
CO harmonic frequency / cm^{-1}	1934.0 ± 0.6	1946.1± 0.4	1970.2 ± 0.4
CO anharmonicity constant / $x10^{-3}$	6.45 ± 0.09	6.31 ± 0.06	6.49 ± 0.06
CO force constant / N m^{-1}	1511.87 ± 0.02	1530.93 ± 0.02	1569.08 ± 0.02
CO dissociation energy / kJ mol^{-1}	897 ± 1	922 ± 9	908 ± 9

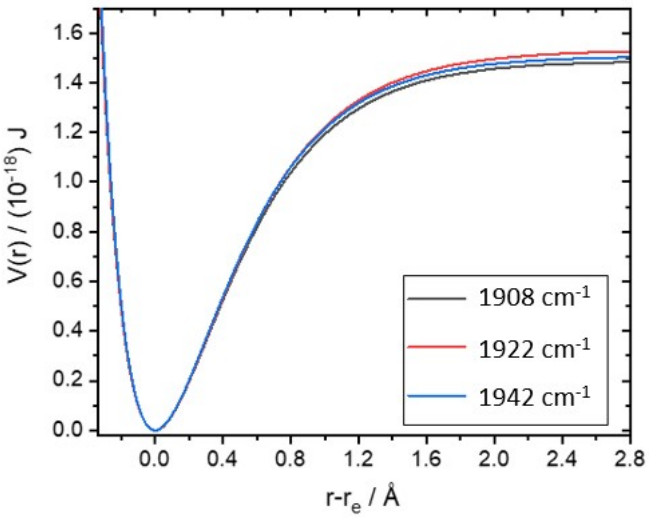

Figure S8: Morse potentials determined for the CO stretching modes of *Ec*Hyd-1 active site states with fundamental frequencies at 1908 (black), 1922 (red) and 1942 cm^{-1} (blue) respectively.

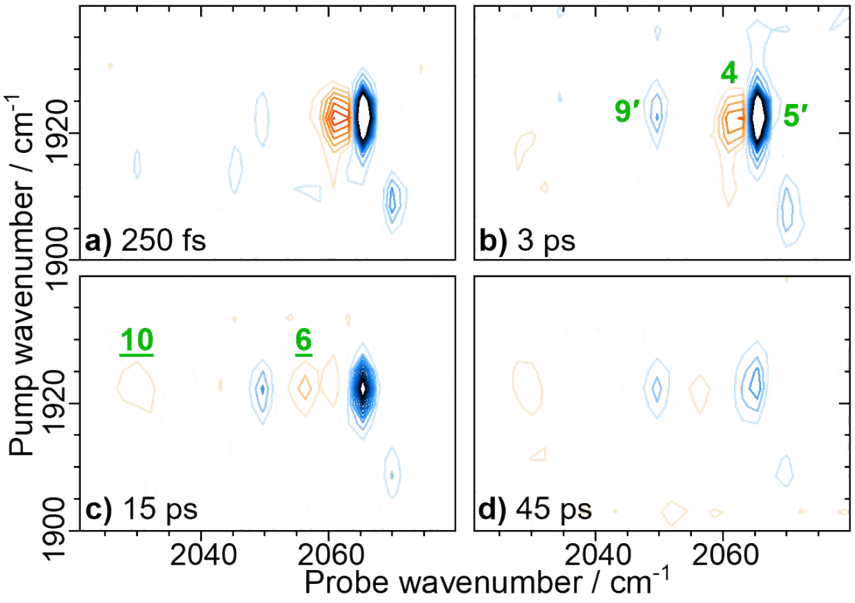

Figure S9: Magnification of the 2D-IR spectrum of as-isolated *Ec*Hyd-1 for pump frequencies coinciding with ν_{CO} bands and probe frequencies coinciding with ν_{CN-} bands at a series of values of T_w. to show energy transfer peaks, 6 and 10. **a)** T_w = 250 fs, **b)** T_w = 3 ps, **c)** T_w = 15 ps **d)** T_w = 45 ps.

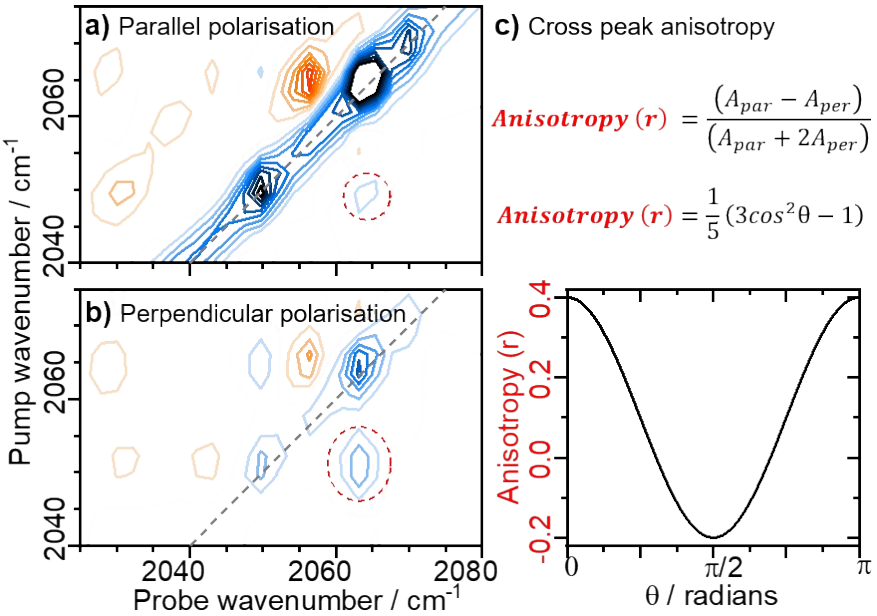

Figure S10 :2D-IR spectra of as-isolated *Ec*Hyd-1 recorded at a T_w of 250 fs with **(a)** perpendicular and **(b)** parallel polarisation. The spectra show the CN-pump, CN-probe quadrant displayed with the same signal scaling. The amplitude of the peak, indicated by the red dashed circle, was used along with the displayed equation **(c)** to determine the angle between the transition dipole moments of the coupled CN bands.[7]

Table S2: Vibrational lifetimes for the carbonyl and cyanide modes. (± values indicate standard deviation derived from fitting).

CO frequency (cm^{-1})	CO lifetime (ps)	CN1 frequency (cm^{-1})	CN1 lifetime (ps)	CN2 frequency (cm^{-1})	CN2 lifetime (ps)
1908	16±3			2070	29±2
1923	17±2	2063	37±2	2050	32±2
1942	25±3	2092	41±4	2080	40±2
1948		2097	49±5	2080	40±2

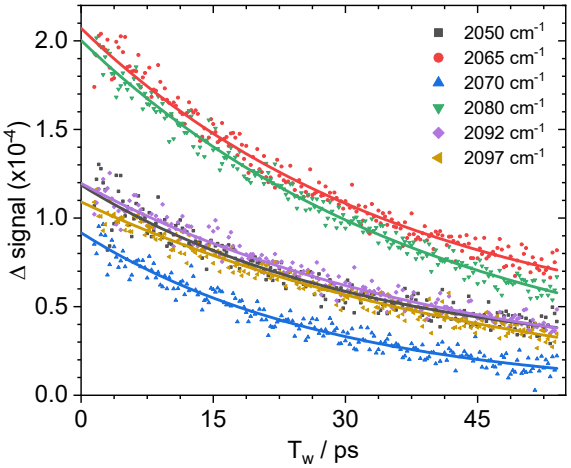

Figure S11: Dynamics of the v=0-1 transitions of CN^- stretching modes of *Ec*Hyd-1 (points) and results of fitting the data to mono-exponential functions (solid lines).

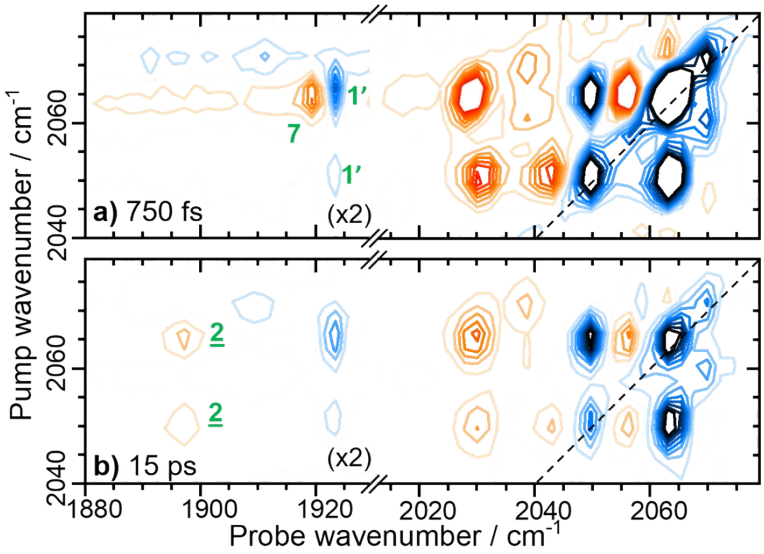

Figure S12: Magnification of the 2D-IR spectrum of as-isolated *Ec*Hyd-1 for pump frequencies coinciding with ν_{CN} bands at values of T_w. **a)** T_w = 750 fs; **b)** T_w = 15 ps showing energy transfer peaks, 2.

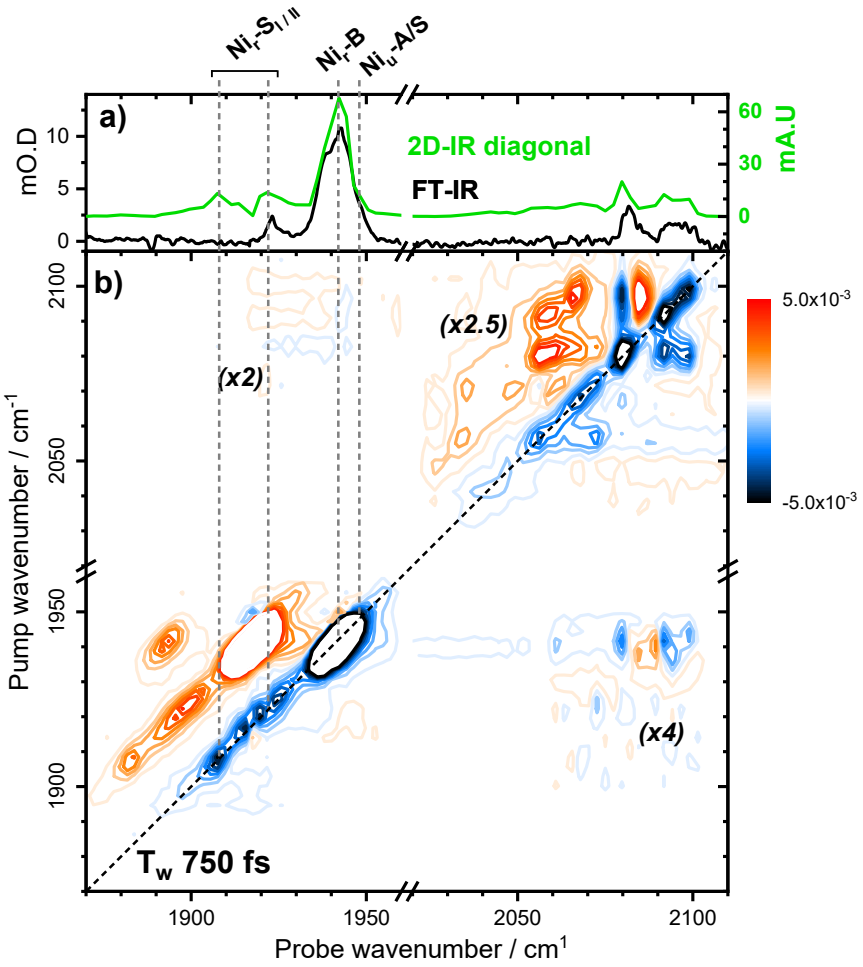

Figure S13 (a) IR absorption spectrum of O_2-oxidised *Ec*Hyd-1 (black trace) and projection of the 2D-IR spectrum diagonal (green). The negative signals of the diagonal have been inverted for comparison with the IR absorption spectrum. **(b)** 2D-IR spectrum of oxidised EcHyd-1 recorded at a waiting time (T_w) of 750 fs. The black dashed line indicates the spectrum diagonal. The grey dashed lines indicate the ν_{CO} modes for each of the active site states present. Numbers in brackets indicate the magnification of the three quadrants of the 2D-IR spectrum containing peaks due to ν_{CN} modes in relation to the ν_{CO} region of the spectrum (1900 - 1950 cm^{-1}), which contains the most intense peaks.

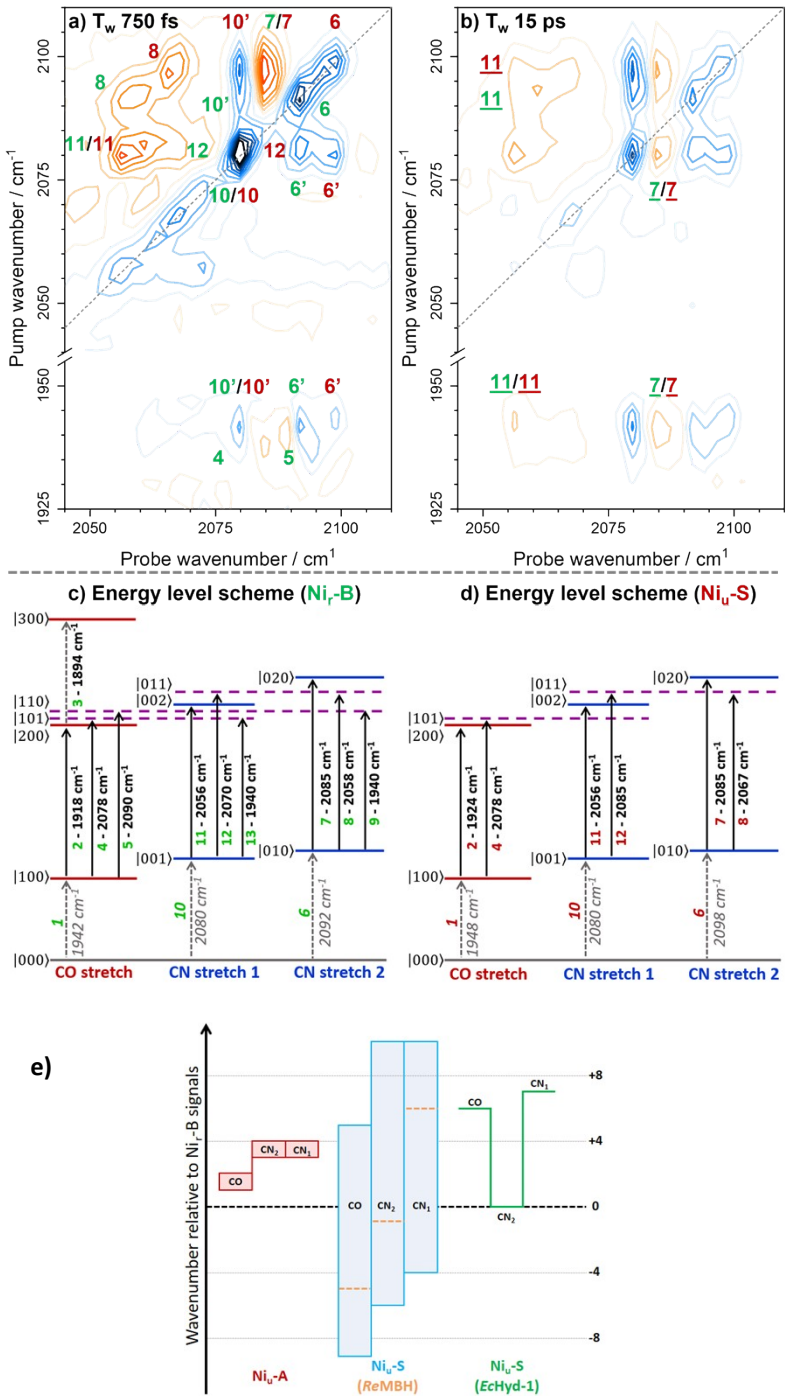

Figure S14 Magnification of the 2D-IR spectrum of O_2-oxidised *Ec*Hyd-1 for probe frequencies coinciding with ν_{CN} bands at a T_w of **a)** 750 fs and **b)** 15ps. **(c** and **d)** Energy level diagrams showing vibrational energy levels $|\nu_{CO}\nu_{CN1}\nu_{CN2}\rangle$ and transition energies of the ν_{CO} and ν_{CN} vibrational manifold, as detected for the active site state of *Ec*Hyd-1 with a ν_{CO} fundamental frequency of 1942 cm^{-1} **(c)** and 1948 cm^{-1} **(d)**. Transitions are labelled with numbers used to identify peak assignments in the 2D-IR spectra. Corresponding frequencies are reported on the arrows. **(e)** Diagram showing the wavenumbers reported for CO, CN_1 and CN_2 stretching modes of NiFe-hydrogenases (*Dv*MF, *Av*MBH, *Dg*MBH and *Re*MBH) in the Ni_u-A (red) and Ni_u-S (blue) states relative to Ni_r-B signals from the same enzyme. Relative wavenumbers for the Ni_u-S states of *Re*MBH and *Ec*Hyd-1 are shown as orange dashed and solid green lines, respectively.

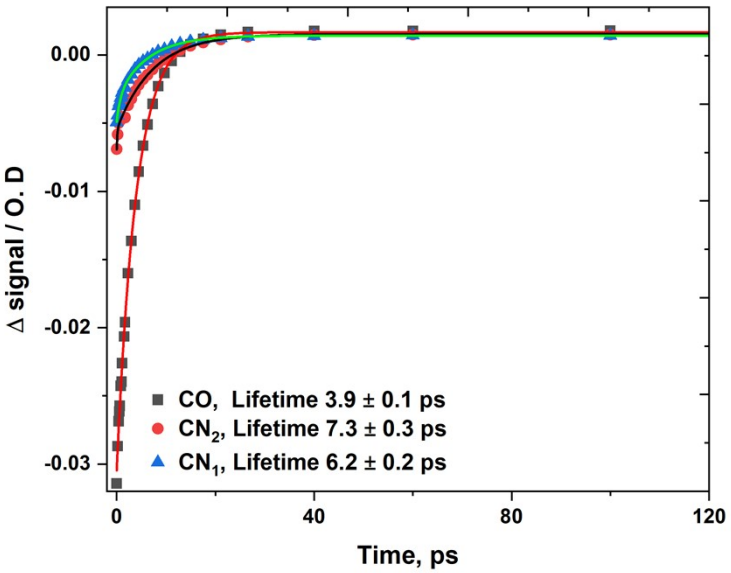

Figure S15: Relaxation dynamics of v=0-1 signals of the CO and CN^- stretching modes of compound **M1** in H_2O (points) and fitting to mono-exponential functions (solid lines).

Table S3: Single and mixed mode anharmonicities for the four redox states of *Ec*Hyd-1 and the single one from *Re*RH.

(*Ec*Hyd-1)	CO	CN_2	CN_1
CO (1908 cm^{-1})	**25**	-	2
CN_2 (2059 cm^{-1})	-	**20**	20
CN_1 (2070 cm^{-1})	-	20	**7**

(*Ec*Hyd-1)	CO	CN_2	CN_1
CO (1922 cm^{-1})	**25**	-	2
CN_2 (2050 cm^{-1})	-	**20**	20
CN_1 (2063 cm^{-1})	2	20	**7**

(*Ec*Hyd-1)	CO	CN_2	CN_1
CO (1942 cm^{-1})	**24**	2	2
CN_2 (2080 cm^{-1})	2	**24**	22
CN_1 (2092 cm^{-1})	2	22	**7**

(*Ec*Hyd-1)	CO	CN_2	CN_1
CO (1948 cm^{-1})	**24**	2	-
CN_2 (2080 cm^{-1})	-	**24**	13
CN_1 (2098 cm^{-1})	-	13	**13**

(*Re*RH)	CO	CN_2	CN_1
CO (1943 cm^{-1})	**25**	-	-
CN_2 (2071 cm^{-1})	-	**18**	24
CN_1 (2080 cm^{-1})	-	24	**8**

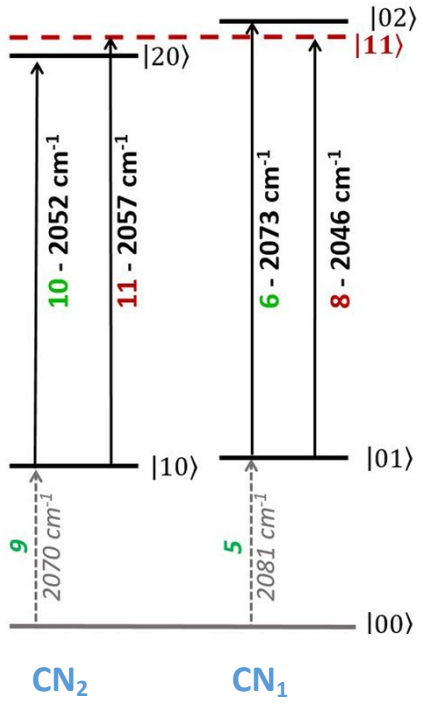

Figure S16: Energy level diagram showing vibrational energy levels $|v_{CN1}\ v_{CN2}\rangle$ and transition energies of the v_{CN} vibrational manifold, as detected for the active site state of *Re*RH. Transitions are labelled with numbers used to identify peak assignments in the 2D-IR spectra. Corresponding frequencies are reported on the arrows.

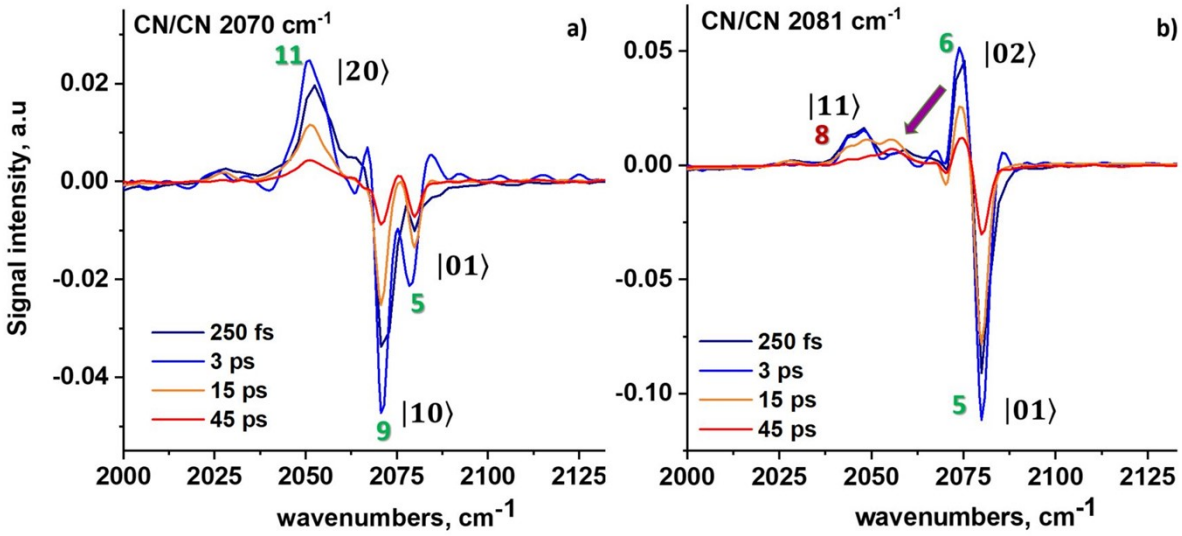

Figure S17: Slices from the 2DIR spectra of *ReRH* measured at different T_w at pump frequencies of **a)** 2070 cm^{-1} and **b)** 2081 cm^{-1}. Peak assignments follow the corresponding energy level diagram showed in Figure S14. The purple arrow highlights the appearance of the energy transfer peak at later waiting times (visible for the 15 ps and 45 ps trace but not at earlier times).

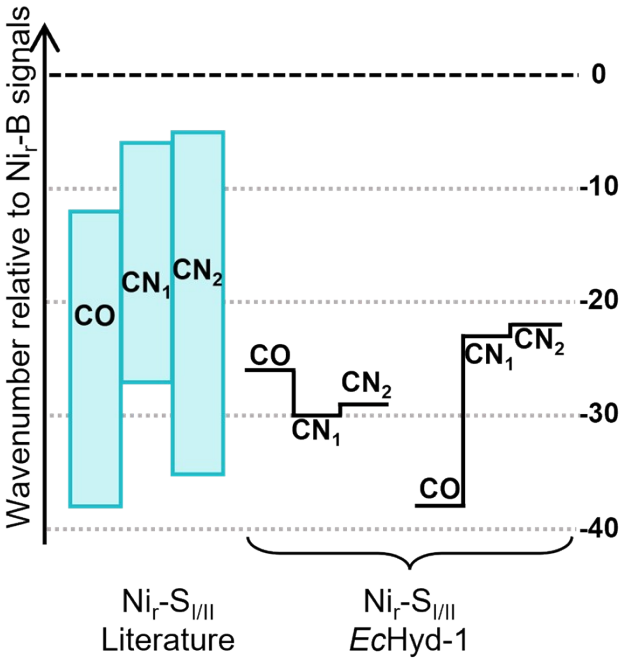

Figure S18: Diagram showing the wavenumbers reported for CO, CN_1 and CN_2 stretching modes of NiFe-hydrogenases (*Dv*MF, *Av*MBH, *Dg*MBH and *Re*MBH,[8-11]) in the Ni_r-S states (blue) relative to Ni_r-B signals from the same enzyme.

References

(1) Flanagan, L. A.; Wright, J. J.; Roessler, M. M.; Moir, J. W.; Parkin, A. Re-Engineering a NiFe Hydrogenase to Increase the H 2 Production Bias While Maintaining Native Levels of O 2 Tolerance. *Chem. Commun.* **2016**, *52* (58), 9133–9136.

(2) Hunt, N. T.; Greetham, G. M.; Towrie, M.; Parker, A. W.; Tucker, N. P. Relationship between Protein Structural Fluctuations and Rebinding Dynamics in Ferric Haem Nitrosyls. *Biochem. J.* **2011**, *433* (3), 459–468.

(3) Adamson, H.; Robinson, M.; Wright, J. J.; Flanagan, L. A.; Walton, J.; Elton, D.; Gavaghan, D. J.; Bond, A. M.; Roessler, M. M.; Parkin, A. Retuning the Catalytic Bias and Overpotential of a [NiFe]-Hydrogenase via a Single Amino Acid Exchange at the Electron Entry/Exit Site. *J. Am. Chem. Soc.* **2017**, *139* (31), 10677–10686.

(4) Schink, B.; Schlegel, H. G. The Membrane-Bound Hydrogenase of Alcaligenes Eutrophus. I. Solubilization, Purification, and Biochemical Properties. *Biochim. Biophys. Acta - Enzymol.* **1979**, *567* (2), 315–324.

(5) Bernhard, M.; Schwartz, E.; Rietdorf, J.; Friedrich, B. The Alcaligenes Eutrophus Membrane-Bound Hydrogenase Gene Locus Encodes Functions Involved in Maturation and Electron Transport Coupling. *J. Bacteriol.* **1996**, *178* (15), 4522–4529.

(6) Volbeda, A.; Darnault, C.; Parkin, A.; Sargent, F.; Armstrong, F. A.; Fontecilla-Camps, J. C. Crystal Structure of the O 2 -Tolerant Membrane-Bound Hydrogenase 1 from Escherichia Coli in Complex with Its Cognate Cytochrome B. *Structure* **2013**, *21* (1), 184–190.

(7) Golonzka, O.; Tokmakoff, A. Polarization-Selective Third-Order Spectroscopy of Coupled Vibronic States. *J. Chem. Phys.* **2001**, *115* (1), 297–309.

(8) Tai, H. L.; Xu, L. Y.; Inoue, S.; Nishikawa, K.; Higuchi, Y.; Hirota, S., Photoactivation of the Ni-SIr state to the Ni-SIa state in NiFe hydrogenase: FT-IR study on the light reactivity of the ready Ni-SIr state and as-isolated enzyme revisited. *PCCP* **2016,** *18* (32), 22025-22030.

(9) Bleijlevens, B.; van Broekhuizen, F. A.; De Lacey, A. L.; Roseboom, W.; Fernandez, V. M.; Albracht, S. P. J., The activation of the NiFe -hydrogenase from Allochromatium vinosum. An infrared spectro-electrochemical study. *Journal of Biological Inorganic Chemistry* **2004,** *9* (6), 743-752.

(10) deLacey, A. L.; Hatchikian, E. C.; Volbeda, A.; Frey, M.; FontecillaCamps, J. C.; Fernandez, V. M., Infrared spectroelectrochemical characterization of the NiFe hydrogenase of Desulfovibrio gigas. *Journal of the American Chemical Society* **1997,** *119* (31), 7181-7189.

(11) Saggu, M.; Zebger, I.; Ludwig, M.; Lenz, O.; Friedrich, B.; Hildebrandt, P.; Lendzian, F., Spectroscopic Insights into the Oxygen-tolerant Membrane-associated NiFe Hydrogenase of Ralstonia eutropha H16. *Journal of Biological Chemistry* **2009,** *284* (24), 16264-16276.